Comparison of the *pn* quasiparticle RPA and shell model for Gamow-Teller beta and double-beta decays

Liang Zhao* and B. Alex Brown

National Superconducting Cyclotron Laboratory and Department of Physics and Astronomy, Michigan State University, East Lansing, Michigan 48824

(Received 24 August 1992)

We examine the validity of the *pn* quasiparticle RPA (*pn*QRPA) as a model for calculating β^+ and $2\nu\beta\beta$ Gamow-Teller decays by making a comparison of the *pn*QRPA with a large-basis shell-model calculation within the $0f1p$ shell. We employ A=46 nuclei (those with six valence nucleons) for this comparison. Our comparison includes the decay matrix elements summed over final states, the strength distributions, and, for the first time, the coherent transition matrix elements (CTME). The *pn*QRPA overestimates the total β^+ and $2\nu\beta\beta$ matrix elements. There are large differences in the shape of the spectra as well as in the CTME between the *pn*QRPA and shell-model results. Empirical improvements for the *pn*QRPA are discussed.

PACS number(s): 21.60.Cs, 21.60.Jz

I. INTRODUCTION

The beta (β) decay process was one of the first types of radioactivity to be observed and still provides new valuable insight into weak interactions and nuclear structure [1, 2]. Nuclear double-beta ($\beta\beta$) decay phenomena is a rare transition between two nuclei of the same mass number having a change of two units of nuclear charge. In cases of interest, ordinary single beta decay is forbidden because of energy conservation or because of very strong suppression due to a large angular momentum mismatch between the parent and daughter states. There are two modes of double-beta decay [3–6],

$$2\ \nu \text{ mode}: (A, Z) \rightarrow (A, Z+2) + 2e^- + 2\bar{\nu},$$

$$0\ \nu \text{ mode}: (A, Z) \rightarrow (A, Z+2) + 2e^-.$$

The first one is called two-neutrino (2ν) $\beta\beta$ decay, which involves the emission of two antineutrinos and two electrons (2ν mode), it occurs in second order in the standard weak interaction theory. Another is called neutrinoless (0ν) $\beta\beta$ decay, which involves the emission of two electrons and no neutrinos. This process violates the lepton number conservation and requires the neutrino to be a Majorana particle and have a nonzero mass and/or a nonstandard right-hand coupling [3–6]. It occurs in some theories beyond the standard weak interaction model [3–6]. The $2\nu\beta\beta$ decay has been observed in recent experiments [7–10], but the $0\nu\beta\beta$ decay has not yet been observed.

There are two important nuclear models which have been applied to the study of β and $\beta\beta$ decays, the shell model and the proton-neutron quasiparticle random phase approximation (*pn*QRPA). Present shell-model theory, namely, the large-basis shell model [11], assumes that the nuclear structure properties are determined by the valence nucleons which simultaneously occupy several different, partially filled, single-particle states. Thus the large-basis shell-model calculation takes into account many multinucleon configurations. Many experimental data for light nuclei ($A \leq 40$) can be successfully explained and even predicted by the large-basis shell-model calculations [1, 11]. However, the dimension of the Hamiltonian matrix increases rapidly when the single-particle basis increases and the large-basis shell model calculation becomes computationally impractical for most cases of interest with $A > 60$.

The *pn*QRPA was introduced by Halbeib and Sorensen [12] and further developed by Cha [13]. In this model, the excitations are constructed by acting two-quasiparticles creation and destruction operators on a ground state which is given by the BCS. The dimensions involved in the *pn*QRPA are relatively small so that it can be employed to study the β and $\beta\beta$ decays in all nuclei. In recent years, the *pn*QRPA has been used to calculate the Gamow-Teller transition strength in β and $\beta\beta$ in light and heavy nuclei [14–20]. Several authors have investigated the particle-particle interaction term which was reintroduced by Cha [13], and found that the β^+ transition matrix elements and the $2\nu\beta\beta$ decay matrix elements are sensitive to this term [13, 15]. The total Gamow-Teller transitions strength and the $2\nu\beta\beta$ decay matrix elements are suppressed when the strength of the particle-particle interaction is increased [15–21].

There may be some correlations that could be important in β^+ and $2\nu\beta\beta$ decay which are not included in the *pn*QRPA. Therefore it is very important to examine the validity and accuracy of the *pn*QRPA. These tests can be achieved by making a comparison of the *pn*QRPA and large-basis shell-model calculations in the nuclear mass regions where the large-basis shell-model calculations are possible. The large-basis shell-model calculations include all types of correlations within a given set of single-particle states. Comparisons are most mean-

*Present address: Department of Biochemistry and Biophysics and Cardiovascular Research Institute, School of Medicine, University of California, San Francisco, CA 94143.

ingful if the pnQRPA and shell-model calculations are performed in the same model space and use the same effective interaction.

This kind of comparison for β^+ decay has been made by Lauritzen [21] for several $1s0d$ shell nuclei: Brown and Zhao [22] for ^{28}Mg, Civitarese *et al.* [23] for ^{26}Mg, and Auerbach *et al.* [24] for ^{26}Mg and ^{54}Fe. Lauritzen, Auerbach, Brown, and Zhao concluded that the pnQRPA does not include some important correlations in β^+ decay and fails to reproduce the shell-model results. But Civitarese *et al.* appeared to contradict this conclusion.

In 1989, Brown and Zhao [22] made a comparison of the pnQRPA and large-basis shell-model calculations for hypothetical $\beta\beta$ decay of ^{28}Mg in the $1s0d$ shell. Later Muto *et al.* [25] presented a similar comparison for the $\beta\beta$ decay of ^{48}Ca. But in their work, the model spaces of the pnQRPA and the shell model are not the same: the former is the $(1s0d + 0f1p0g)$ shells, and the latter is the $0f1p$ shell only. Therefore the comparison is confused because a meaningful comparison requires that the calculations of these models are performed in the same model space.

In this work, we will make a comparison of the pnQRPA and large-basis shell model within the $0f1p$ shell. We employ A=46 nuclei (those with six valence nucleons) for this comparison. It is also computationally possible to carry out the full-basis calculation [26] or the nearly full-basis calculation [27] for the experimentally interesting case of ^{48}Ca $\beta\beta$ decay. However, the case of ^{48}Ca $\beta\beta$ decay with a semiclosed neutron shell for an initial state is somewhat different from the typical $\beta\beta$ decay cases in heavier nuclei where both proton and neutron shells are open. Instead we concentrate here on the case of ^{46}Ca $\beta\beta$ decay because both proton and neutron shells are open, and hence it may be more representative of the situation in heavier nuclei in which the pnQRPA has been extensively applied and where the large-basis shell-model calculations of the type discussed here are computationally prohibitive. Since our large-basis shell-model calculations are in good agreement with experiment in the case of A=48 [27], for A=46, in the absence of actual experimental data, we will take the results of the large-basis shell-model calculations to be equivalent to "experiment" for the purpose of the present comparison to the pnQRPA.

Our comparison not only concentrates on the Gamow-Teller strength summed over all final states and/or their distributions, but also investigates the relative single-particle state contributions. The state-dependent gap equation in the BCS is used in our study. Some empirical improvements for the pnQRPA are discussed as well.

This paper is organized as follows. In Sec. II, the BCS and pnQRPA equations are developed and the coherent transition matrix element (CTME), which describes the single-particle state contribution to the total strength, is introduced. Our comparison of the pnQRPA and shell model for β and $2\nu\beta\beta$ decays is presented in Secs. III A and III B, respectively. In Sec. IV, a few possible improvements of the pnQRPA are discussed. In Sec. V, we give the summary and conclusions. In the Appendix, the coherent transition matrix element is discussed.

II. FORMALISM

A. pnQRPA equations

We start with the equation of motion [28,29], where the excited eigenstates $|m\rangle$ are constructed from the phonon creation operator $Q_m^\dagger$ which is defined by

$$|m\rangle = Q_m^\dagger|0\rangle, \quad \text{and } Q_m|0\rangle = 0, \quad \text{for all } m \tag{1}$$

where $|m\rangle$ and $|0\rangle$ are the excited eigenstates and the physical ground state. They satisfy the Schrödinger equation,

$$H|m\rangle = E_m|m\rangle \text{ and } H|0\rangle = E_0|0\rangle. \tag{2}$$

Then one obtains the following equation of motion from the above relations;

$$[H, Q_m^\dagger]|0\rangle = (E_m - E_0)Q_m^\dagger|0\rangle. \tag{3}$$

Multiplying from the left with an arbitrary state of the form $\langle 0|\delta Q_m$, we get

$$\langle 0|[\delta Q_m, [H, Q_m^\dagger]]|0\rangle = \hbar\omega\langle 0|[\delta Q_m, Q_m^\dagger]|0\rangle, \tag{4}$$

where $\hbar\omega = E_m - E_0$.

In order to obtain the pnQRPA equation, the phonon creation operators in the angular momentum coupled representation are written as [12, 13, 21]

$$Q_m^\dagger(J,M) = \sum_{p,n}[X_m^{pn}\mathcal{A}_{pn}^\dagger(pn,JM) - Y_m^{pn}\tilde{\mathcal{A}}_{pn}(pn,JM)], \tag{5}$$

$$\mathcal{A}_{pn}^\dagger(pn,JM) = \sum_{m_p,m_n}\langle j_p m_p j_n m_n|JM\rangle c_{p,m_p}^\dagger c_{n,m_n}^\dagger, \tag{6}$$

$$\tilde{\mathcal{A}}_{pn}(pn,JM) = (-1)^{J+M}\mathcal{A}_{pn}(pn,J-M), \tag{7}$$

where $c_{p(n),m_{p(n)}}^\dagger$ is the quasiproton (quasineutron) creation operator. The labels p/n stand for (nlj) for the proton/neutron single-particle states. In terms of the spherical shell-model states, the particle and quasiparticle creation and destruction operators are related by the Bogoliubov transformation, e.g., for proton

$$c_{p,m_p}^\dagger = u_p a_{p,m_p}^\dagger + (-)^{j_p+m_p}v_p a_{p,-m_p}, \tag{8}$$

where $u_p^2 + v_p^2 = 1$, and $a_{p,m_p}^\dagger$ is the proton creation operator for the single-particle state. v_p^2 turns out to be the proton occupation probability. The eigenvalue $\hbar\omega$ and the forward- and backward-going amplitudes X and Y are obtained by solving the pnQRPA equation

$$\begin{pmatrix} A & B \\ -B^* & -A^* \end{pmatrix}\begin{pmatrix} X \\ Y \end{pmatrix} = \hbar\omega\begin{pmatrix} X \\ Y \end{pmatrix}, \tag{9}$$

with the orthogonality relation

$$\sum_{pn}[X_m^{pn}X_{m'}^{pn} - Y_m^{pn}Y_{m'}^{pn}] = \delta_{mm'}. \tag{10}$$

The matrix elements A and B are explicitly given by [12,13,15,21]

$$A^J_{pnp'n'} = \langle \mathrm{QRPA}|[\mathcal{A}_{pn}(pn,JM),[H,\mathcal{A}^\dagger_{pn}(p'n',JM)]]|\mathrm{QRPA}\rangle$$
$$\simeq \langle \mathrm{BCS}|[\mathcal{A}_{pn}(pn,JM),[H,\mathcal{A}^\dagger_{pn}(p'n',JM)]]|\mathrm{BCS}\rangle$$
$$= (E_p+E_n)\delta_{pp'}\delta_{nn'} + (H^{pn}_{22})^J_{pnp'n'}, \quad (11)$$
$$B^J_{pnp'n'} = \langle \mathrm{QRPA}|[\mathcal{A}_{pn}(pn,JM),[H,\tilde{\mathcal{A}}_{pn}(p'n',JM)]]|\mathrm{QRPA}\rangle$$
$$\simeq \langle \mathrm{BCS}|[\mathcal{A}_{pn}(pn,JM),[H,\tilde{\mathcal{A}}_{pn}(p'n',JM)]]|\mathrm{BCS}\rangle$$
$$= -(G^{pn})^J_{pnp'n'}, \quad (12)$$

with

$$(H^{pn}_{22})^J_{pnp'n'} = g_{pp}V^J_{pnp'n'}(u_pu_nu_{p'}u_{n'} + v_pv_nv_{p'}v_{n'}) + g_{ph}W^J_{pnp'n'}(u_pv_nu_{p'}v_{n'} + v_pu_nv_{p'}u_{n'}), \quad (13)$$
$$(G^{pn})^J_{pnp'n'} = g_{pp}V^J_{pnp'n'}(u_pu_nv_{p'}v_{n'} + v_pv_nu_{p'}u_{n'}) - g_{ph}W^J_{pnp'n'}(v_pu_nu_{p'}v_{n'} + u_pv_nv_{p'}u_{n'}), \quad (14)$$

where $|\mathrm{QRPA}\rangle$ is the QRPA ground state. The quasiproton and quasineutron energies E_p and E_n and occupation factors u, v are obtained by solving the BCS equation in Sec. II B. The matrix elements of the particle-particle (V) and particle-hole (W) interaction are related by Pandya transformation,

$$W^J_{pn,p'n'} = -(-1)^{j_p+j_n+j_{p'}+j_{n'}} \times \sum_{J'}(2J'+1)\begin{Bmatrix} j_p & j_n & J \\ j'_p & j'_n & J' \end{Bmatrix} V^{J'}_{pn',p'n}. \quad (15)$$

In order to discuss the results as a function of the strength associated with each part of the interaction, the multiplicative factors g_{ph} and g_{pp} are conventionally introduced for the particle-particle and particle-hole, respectively. They are both equal to unity in the standard pnQRPA theory.

The charge-exchange transition matrix elements of the Gamow-Teller operator between the ground state $|J^\pi_i\rangle$ and the excited state $|J^\pi_m\rangle$ are given by

$$B(\mathrm{GT}) = \frac{1}{2J_i+1}(\langle J^\pi_m||\sigma t||J^\pi_i\rangle)^2, \quad (16)$$

where $J^\pi_m = 1^+_m$ and $J^\pi_i = 0^+_i$ in our example. We denote

$$M_m(\mathrm{GT}) = \langle J^\pi_m||\sigma t||J^\pi_i\rangle, \quad (17)$$

where σ is the Pauli spin operator. The isospin operator t can be the raising or lowering operator, t^+ or t^-, corresponding to β^+ and β^- Gamow-Teller transitions, respectively. In the pnQRPA, one obtains

$$M_m(\mathrm{GT}^-) = \sum_{pn}\langle p||\sigma||n\rangle(X^{pn}_m u_pv_n + Y^{pn}_m v_pu_n), \quad (18)$$
$$M_m(\mathrm{GT}^+) = -\sum_{pn}\langle p||\sigma||n\rangle(X^{pn}_m v_pu_n + Y^{pn}_m u_pv_n). \quad (19)$$

The above equations for $M_m(\mathrm{GT})$ in the pnQRPA can be rewritten as,

$$M_m(\mathrm{GT}) = \sum_{pn}\langle p||\sigma||n\rangle \mathrm{OBTD}(p,n,m,i)_{\mathrm{QRPA}}, \quad (20)$$

where the $\mathrm{OBTD}(p,n,m,i)_{\mathrm{QRPA}}$ is a one-body transition density. The Gamow-Teller matrix elements summed over all final states, J^π_m, satisfy the sum rule,

$$\sum B(\mathrm{GT}^-) - \sum B(\mathrm{GT}^+) = 3(N-Z). \quad (21)$$

B. BCS equations

In the BCS approximation, the quasiproton energies E_p, occupation probabilities v^2_p, and pairing gaps Δ_p are given by [30]

$$E_p = \sqrt{(\varepsilon_p - \lambda_\pi)^2 + \Delta^2_p}, \quad (22)$$
$$v^2_p = \frac{1}{2}\left(1 - \frac{\varepsilon_p - \lambda_\pi}{\sqrt{(\varepsilon_p-\lambda_\pi)^2+\Delta^2_p}}\right), \quad (23)$$
$$\Delta_p = -\sum_{p'}\sqrt{\frac{2j_{p'}+1}{2j_p+1}}u_{p'}v_{p'}V^{J=0}_{pp,p'p'}, \quad (24)$$

where λ_π is the proton Fermi energy, ε_p is the single proton energy and $V_{pp,p'p'}$ is the proton two-body interaction. The above equations are solved with the constraint for the total proton number

$$N_\pi = \sum_p(2j_p+1)v^2_p, \quad (25)$$

to determine the constant λ_π. A similar set of the equations is solved for neutrons. The single proton energies ε_p are related to the bare single-particle proton energies ε^0_p at the closed shell by addition of the rearrangement terms Γ_p

$$\varepsilon_p = \hat{\varepsilon}^0_p + \Gamma_p, \quad (26)$$

where

$$\Gamma_p = \frac{1}{2j_p+1}\sum_{p'}(1+\delta_{pp'})v^2_{p'}\sum_J(2J+1)V^J_{pp',pp'} + \frac{1}{(2j_p+1)}\sum_{n'}v^2_{n'}\sum_J(2J+1)V^J_{pn',pn'}. \quad (27)$$

The first term refers to like particle correction and the second term to unlike particle correction. The rearrangement term for ε_n has the same form but with the p/n indices interchanged. The BCS Eqs. (22)–(25) plus the

rearrangement terms can be solved iteratively.

We note that the input ingredients in the BCS [Eqs. (9)–(14)] and the *pn*QRPA [Eqs. (22)–(27)], in our formalism, are consistent with those in the shell model, namely, the bare single particle energies ε_j^0 at the closed shell and two-body interaction matrix elements V_{ijkl}^J. The Coulomb shift is taken into account in both shell model and *pn*QRPA in our comparison [31].

C. B(GT) in shell-model calculations

In the shell-model calculation, the Gamow-Teller strength is equal to the product of one-body transition density and single particle matrix element [1], and the matrix element M_m in Eq. (17) is expressed by

$$M_m(\mathrm{GT}) = \sum_{pn} \langle p||\sigma||n\rangle \mathrm{OBTD}(p,n,m,i)_{\mathrm{SM}}, \tag{28}$$

where

$$\mathrm{OBTD}(p,n,m,i)_{\mathrm{SM}} = \langle J_m^\pi || \frac{[a_p^+ \otimes \tilde{a}_n]^{\Delta J}}{\sqrt{2\Delta J+1}} || J_i^\pi \rangle. \tag{29}$$

The shell model wave function $|J_m^\pi\rangle$ and $|J_i^\pi\rangle$ as well as $\mathrm{OBTD}(p,n,m,i)_{\mathrm{SM}}$ are calculated with the OXBASH shell-model code [32]. The proton (neutron) occupation probabilities in the shell model are given by

$$v_{p(n)}^2(\mathrm{SM}) = \frac{\langle J_i^\pi | a_{p(n)}^+ a_{p(n)} | J_i^\pi \rangle}{2j_{p(n)}+1}, \tag{30}$$

For the Gamow-Teller transitions in our example, we have $|J_m^\pi\rangle = |1_m^+\rangle$, $|J_i^\pi\rangle = |0_i^+\rangle$ and $\Delta J = 1$.

D. The coherent transition matrix elements

The B(GT) spectrum itself lacks information about the single-particle state contributions in the charge-exchange process, because we sum over all single-particle state components p, n in Eqs. (18)–(20) for the *pn*QRPA and Eq. (28) for the shell model. Therefore, we introduce new quantities which can describe such single-particle state contributions to the total strength. We define the *coherent one-body transition density* (COBTD) as

$$\mathrm{COBTD}(p,n,i) = \frac{1}{\sqrt{\sum_m B(\mathrm{GT})}} \sum_m M_m(\mathrm{GT}) \mathrm{OBTD}(p,n,m,i), \tag{31}$$

where M_m(GT) is given by Eq. (17). The OBTD is given by Eqs. (29) and (20) for the shell model and the *pn*QRPA, respectively. Also the *coherent transition matrix element* (CTME) is defined by

$$\mathrm{CTME}(p,n,i) = \langle p||\sigma||n\rangle \mathrm{COBTD}(p,n,i). \tag{32}$$

The COBTD and CTME are a function of the single-particle state components. All final states (m) are summed up in Eq. (31). The relation between the total B(GT) and the CTME is given by

$$\left\{ \sum_{p,n} \mathrm{CTME}(p,n,i) \right\}^2 = \sum_m B(\mathrm{GT}). \tag{33}$$

In the Appendix, we will discuss the derivation of the CTME. The CTME are very useful for observing the microscopic structure of the total (coherent) Gamow-Teller strength which is dependent only upon the structure of the initial state, and this is the first work in which the CTME from the *pn*QRPA and large-basis shell model are compared.

E. Formalism of $2\nu\beta\beta$ decay

In the shell-model calculations, the (intermediate state) energy dependent matrix element is defined by

$$M_{\mathrm{GT}}(E_m) = \sum_{k=1}^{m} \frac{\langle J_f^\pi||\sigma t^-||J_k^\pi\rangle\langle J_k^\pi||\sigma t^-||J_i^\pi\rangle}{E_k - E_i + T_0/2 + m_e c^2}, \tag{34}$$

where E_k are the excitation energies of the intermediate states, E_i is the intial state energy, $T_0/2$ is the Q value of $\beta\beta$ decay, and $m_e c^2$ is the electron mass. The total matrix element for $2\nu\beta\beta$ is given by $M_{\mathrm{GT}} = M_{\mathrm{GT}}(E_m \to \infty)$. The closure matrix element is defined by

$$B_{\mathrm{CLS}}(E_m) = \sum_{m=1}^{E_m} \langle J_f^\pi||\sigma t^-||J_m^\pi\rangle\langle J_m^\pi||\sigma t^-||J_i^\pi\rangle. \tag{35}$$

The total matrix element is given by $B_{\mathrm{CLS}} = B_{\mathrm{CLS}}(E_m \to \infty)$. In our example, $J_i^\pi = 0_i^+$, $J_f^\pi = 0_f^+$, and $J_k^\pi = 1_k^+$.

In the *pn*QRPA calculations, the $\beta\beta$ formulas become more complicated because the summation in Eqs. (34) and (35) involves the product of two transition matrix elements and each one contains the intermediate states of the intermediate nucleus. Of course, in the shell model, the intermediate states in the two transition matrix elements are the same. But in the *pn*QRPA, we recognize that the intermediate states in the two transition matrix elements are different. They depend on which parent nucleus is being considered. Thus a problem arises that the intermediate states resulting from the two different *pn*QRPA calculations are not orthogonal. Of course, they should be the same physically. In order to solve such a mismatch problem, one can introduce an overlap matrix element between any two intermediate states J_k^π and $J_{k'}^\pi$ [17, 19],

$$\langle J_k^\pi | J_{k'}^\pi \rangle = \sum_{pn} (\bar{X}_{k'}^{pn,J^\pi} X_k^{pn,J^\pi} - \bar{Y}_{k'}^{pn,J^\pi} Y_k^{pn,J^\pi}) \tag{36}$$

where k, k' denote two states with eigenvectors (X,Y) and $(\bar{X},\bar{Y})$, which are constructed from intial and final

states, respectively [17,19,33]. Obviously, if (X,Y) and $(\bar{X},\bar{Y})$ are identical, then we have $\langle J_k^\pi | J_{k'}^\pi \rangle = \delta_{kk'}$ [see Eq. (10)]. With the overlap matrix element, Eqs. (34)–(36) can be rewritten as

$$M_{\rm GT}(E_m) = \sum_{k,k'} \frac{\langle 0_f^+ || \sigma t^- || 1_k^+ \rangle \langle 1_k^+ | 1_{k'}^+ \rangle \langle 1_{k'}^+ || \sigma t^- || 0_i^+ \rangle}{E_k - E_i + T_0/2 + m_e c^2}, \tag{37}$$

$$B_{\rm CLS}(E_m) = \sum_{k,k'} \langle 0_f^+ || \sigma t^- || 1_k^+ \rangle \langle 1_k^+ | 1_{k'}^+ \rangle \langle 1_{k'}^+ || \sigma t^- || 0_i^+ \rangle. \tag{38}$$

We note that there is some arbitrariness to the choice of E_k or $E_{k'}$ in the energy denominator.

III. COMPARISON OF THE *pn*QRPA AND SHELL MODEL

A. Comparison for β decay

In this subsection, we compare the results between the *pn*QRPA and large-basis shell model for β^+ decay of ^{46}Ti and β^- decay of ^{46}Ca. The model space is the full $0f1p$ shell and the effective interaction used is MSOBEP [34]. In this interaction the single-particle energies at A=41 are −8.388, −6.459, −1.897, and −4.478 MeV for the $0f_{7/2}, 1p_{3/2}, 0f_{5/2}$, and $1p_{1/2}$ orbitals, respectively. MSOBEP means that a modified-surface one-boson-exchange potential was used. This potential contains central as well as tensor and spin-orbit components. The fitted interaction (six of the potential strengths as well as the four single-particle energies were adjusted) reproduces the binding energies and excitation energies of the low-lying excited states of nuclei with A=41–49 with an rms deviation of 176 keV.

In the BCS equations given by Sec. II B, the pairing gaps and single-particle rearrangement terms are state dependent and are self-consistently calculated. In Tables I and II, the BCS single-particle energies with the addition of rearrangement terms, quasiparticle energies, pairing gaps, and occupation probabilities of ^{46}Ti and ^{46}Ca are presented. The proton pairing gaps are about 40% less than those obtained from the empirical formula $\Delta_p = 12A^{-1/2}$.

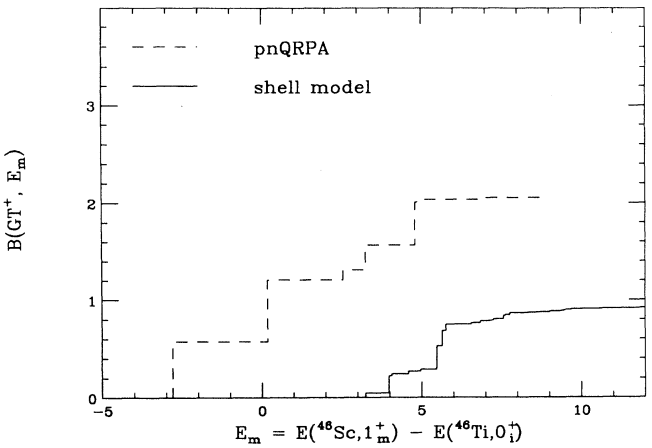

FIG. 1. Running sum of the Gamow-Teller strength $B(\mathrm{GT}^+, E_m)$ for ^{46}Ti $\rightarrow$^{46}Sc as a function of the ^{46}Sc 1^+ excitation energies relative to the ^{46}Ti ground state.

We define the running sum as

$$B(\mathrm{GT}^+, E_m) = \sum_{k=1}^{m} (\langle 1_k^+ || \sigma t^+ || 0_i^+ \rangle)^2, \tag{39}$$

$$B(\mathrm{GT}^-, E_m) = \sum_{k=1}^{m} (\langle 1_k^+ || \sigma t^- || 0_i^+ \rangle)^2. \tag{40}$$

The total $B(\mathrm{GT}^+)$ and total $B(\mathrm{GT}^-)$ are given by $E_m \rightarrow \infty$.

Figures 1 and 2 present the $B(\mathrm{GT}^+, E_m)$ and $B(\mathrm{GT}^-, E_m)$ as a function of the ^{46}Sc 1^+ excitation energy E_m corresponding to the ^{46}Ti and ^{46}Ca ground state, respectively. The *pn*QRPA and shell-model results are shown by dashed and solid lines, respectively.

The J dimensions in our large-basis shell-model calculations are 24, 1514, and 2042 for the ^{46}Ca ground state, the ^{46}Sc 1^+ excitations, and the ^{46}Ti ground state, respectively.

Figure 1 shows three major differences between the results of the *pn*QRPA and the shell model in the β^+ Gamow-Teller strength: (i) the *pn*QRPA calculation does

TABLE I. For ^{46}Ti, proton and neutron single particle energies ε_i (MeV), gap parameters Δ_i (MeV), occupation probabilities v_i^2 and quasiparticle energies E_i (BCS) (MeV) from BCS, the shell-model E_i(SM) and v_i^2(SM). (See text.) The Fermi energies obtained from the BCS calculation are −12.968 MeV and −10.868 MeV for proton and neutron, respectively.

Level	ε_i	Δ_i	v_i^2	E_i(BCS)	E_i(SM)	v_i^2(SM)
$\pi f_{7/2}$	−12.234	1.206	0.239	1.412	1.412	0.187
$\pi p_{3/2}$	−8.194	0.911	0.009	4.861	4.305	0.078
$\pi f_{5/2}$	−5.739	1.314	0.008	7.347	6.845	0.022
$\pi p_{1/2}$	−5.994	0.874	0.004	7.028	6.431	0.031
$\nu f_{7/2}$	−10.809	1.447	0.480	1.448	1.414	0.404
$\nu p_{3/2}$	−6.852	1.104	0.018	4.164	3.336	0.092
$\nu f_{5/2}$	−4.044	1.574	0.013	7.003	6.099	0.054
$\nu p_{1/2}$	−4.553	1.069	0.007	6.405	5.564	0.040

TABLE II. For ^{46}Ca, neutron single particle energies ε_i (MeV), gap parameters Δ_i (MeV), and occupation probabilities v_i^2 and quasineutron energies E_i (MeV) from BCS, the shell-model E_i(SM), v_i^2(SM) (see text). The neutron Fermi energy is −8.712 MeV.

Level	ε_i	Δ_i	v_i^2	E_i	E_i(SM)	v_i^2(SM)
$\nu f_{7/2}$	− 9.395	1.347	0.726	1.510	1.700	0.703
$\nu p_{3/2}$	− 5.507	1.042	0.025	3.370	3.343	0.049
$\nu f_{5/2}$	− 3.354	1.455	0.013	5.552	6.377	0.025
$\nu p_{1/2}$	− 3.107	1.026	0.008	5.698	5.830	0.016

not give sufficient suppression for the total $B(\mathrm{GT}^+)$; (ii) the energies of the first excited state in the two models differ by about 6 MeV; (iii) the strength distributions in two models are mismatched. The shell-model Gamow-Teller strength is mainly concentrated at its low-excitation energy, but in the *pn*QRPA, the strength distribution is much broader.

The coherent transition matrix elements (CTME) defined by Sec. II D are given in Table III for the *pn*QRPA and shell model (see columns A and E). There are significant differences between the two models. Most importantly, the CTME values in the *pn*QRPA and shell model have the opposite sign for the $f_{7/2} \rightarrow f_{7/2}$.

For ^{46}Ca, there is no valence proton in the $0f1p$ shell (i.e., $v_p = 0$), so the matrix B in the *pn*QRPA is zero and the *pn*QRPA reduces to the *pn*QTDA, where the amplitudes Y are equal to zero. In this case, the β^+ transition strength of ^{46}Ca vanishes and the total $B(\mathrm{GT}^-)$ strength is equal to 18 because of the sum rule Eq. (21). In Fig. 2, the first 1^+ eigenvalue of the *pn*QRPA differs by about 5 MeV from that of the shell model.

B. Comparison for $2\nu\beta\beta$ decay

In this subsection, we compare the results of the *pn*QRPA and large-basis shell model for the $2\nu\beta\beta$ of ^{46}Ca. In this case, the initial (final) nucleus has 0 (2) protons and 6 (4) neutrons in the $0f1p$ shell. The double-beta decay matrix elements M_{GT} and/or B_{CLS} consist of the virtual decay routes, β^- and β^+ decays. Their Gamow-Teller strengths in the *pn*QRPA and shell model were presented and discussed in the last section.

In Figs. 3 and 4, we present the running sum of matrix element $B_{\mathrm{CLS}}(E_m)$ and $M_{\mathrm{GT}}(E_m)$ as a function of the 1^+ excitation energies corresponding to the ^{46}Ca ground state. The excitation energies are obtained from the *pn*QRPA calculation for $^{46}\mathrm{Ca} \rightarrow {}^{46}\mathrm{Sc}$, and are employed to evaluate the energy denominator in Eq. (37), but the first 1^+ state in the *pn*QRPA is shifted to the position of the first 1^+ state in the shell model in order to use a consistent energy denominator to calculate $M_{\mathrm{GT}}(E_m)$. In practice, the first 1^+ state in the $2\nu\beta\beta$ calculation is chosen by using the experimental value [27, 35, 36]. (In our case, the shell model and experiment are essentially the same for the position of the lowest 1^+ state energy.)

Qualitatively the *pn*QRPA and shell-model show a similar shape. There is a cancellation between the matrix elements in the low- and high-lying states. The magnitudes, however, are very different. We find the *pn*QRPA does not provide enough suppression for total M_{GT} and B_{CLS}, which are about three to four times larger than those in the large-basis shell-model calculation. The largest difference in the matrix elements are shown in the low-lying states between the two models. For example, the first $M_{\mathrm{GT}}(E_1)$ and $B_{\mathrm{CLS}}(E_1)$ are almost 5 times larger than the corresponding shell-model results. In the *pn*QRPA, the first $B(\mathrm{GT}^-)$ and $B(\mathrm{GT}^+)$ are dominated by the transition $f_{7/2} \rightarrow f_{7/2}$, but in the shell model, this transition contributes only about 50%.

Finally, in Eqs. (37) and (38), we can also calculate

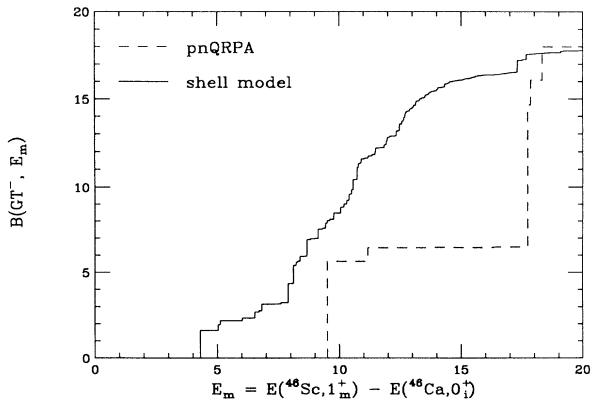

FIG. 2. Running sum of the Gamow-Teller strength $B(\mathrm{GT}^-, E_m)$ for $^{46}\mathrm{Ca} \rightarrow {}^{46}\mathrm{Sc}$ as a function of the ^{46}Sc 1^+ excitation energies relative to the ^{46}Ca ground state.

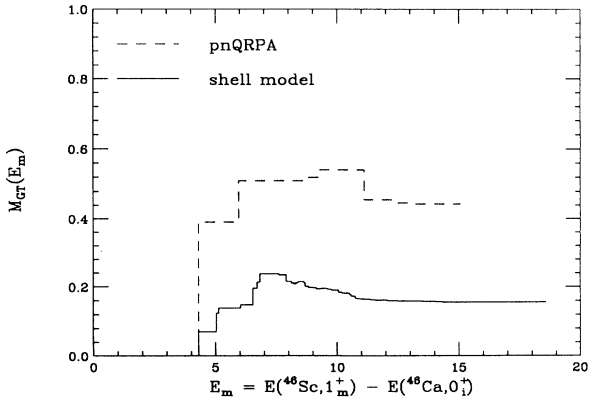

FIG. 3. Running sum of the $2\nu\beta\beta$ decay matrix element $M_{\mathrm{GT}}(E_m)$ as a function of the ^{46}Sc 1^+ excitation energies relative to the ^{46}Ca ground state.

TABLE III. Comparison of the coherent transition matrix elements (CTME) obtained in the *pn*QRPA, "hybrid" *pn*QRPA, and shell-model calculations of ^{46}Ti. A: CTME in the *pn*QRPA with BCS occupation and quasiparticle energies; B: CTME in the *pn*QRPA with BCS occupation and SM quasiparticle energies; C: CTME in the *pn*QRPA with SM occupation and BCS quasiparticle energies; D: CTME in the *pn*QRPA with SM occupation and quasiparticle energies; E: CTME in shell model.

$j_p \rightarrow j_n$	A	B	C	D	E
$f_{7/2} \rightarrow f_{7/2}$	0.108	0.088	0.011	-0.070	-0.308
$f_{7/2} \rightarrow f_{5/2}$	1.641	1.706	1.187	1.223	1.431
$p_{3/2} \rightarrow p_{3/2}$	0.005	0.000	0.199	0.191	0.014
$p_{3/2} \rightarrow f_{5/2}$	0.000	0.000	0.000	0.000	0.000
$p_{3/2} \rightarrow p_{1/2}$	0.011	0.009	0.202	0.206	0.139
$f_{5/2} \rightarrow f_{7/2}$	-0.325	-0.391	-0.353	-0.433	-0.319
$f_{5/2} \rightarrow p_{3/2}$	0.000	0.000	0.000	0.000	0.000
$f_{5/2} \rightarrow f_{5/2}$	-0.002	-0.003	0.016	0.012	0.024
$p_{1/2} \rightarrow p_{3/2}$	-0.006	-0.010	0.028	0.015	-0.020
$p_{1/2} \rightarrow p_{1/2}$	0.000	0.000	0.010	0.011	0.002

the $2\nu\beta\beta$ decay matrix elements by projecting the 1^+ excitations from ^{46}Ca β^- decay onto ones from ^{46}Ti β^+ decay and using the corresponding energy denominators. The results are similar to those discussed above.

C. Sensitivity to the particle-particle interaction

Since the $B(\mathrm{GT}^+)$ strength and $2\nu\beta\beta$ decay matrix elements B_{CLS} and M_{GT} are more sensitive to g_{pp} than to g_{ph}, we will set $g_{ph} = 1$ and discuss the dependence on g_{pp}. In Fig. 5, the $B(\mathrm{GT}^+)$ spectra with various g_{pp} values are presented. We find the *pn*QRPA results are very sensitive to g_{pp}, in agreement with the previous conclusions [13,15,21]. The total shell-model $B(\mathrm{GT}^+)$ is reproduced by the *pn*QRPA with $g_{pp} = 1.4$, but the shapes of the strength distributions of two models are totally different.

When g_{pp} increases beyond a certain value, the lowest eigenvalue becomes the imaginary and the *pn*QRPA equation collapses. It means that the *pn*QRPA theory is no longer a valid model. Around this g_{pp}, the equation gives unrealistic large amplitudes X and Y.

In Figs. 6 and 7, we present $M_{\mathrm{GT}}(E_m)$ and $B_{\mathrm{CLS}}(E_m)$ with respect to various g_{pp} values. The particle-particle interaction suppresses the total matrix elements in agreement with previous studies [16–19]. If the particle-particle channel is shut off ($g_{pp} = 0$), the cancellation of $B_{\mathrm{CLS}}(E_m)$ between the low- and high-lying excitations disappears. However, the cancellation emerges and becomes stronger as g_{pp} is increased.

IV. PHENOMENOLOGICAL IMPROVEMENTS OF *pn*QRPA

We now investigate various ways to understand and then improve the agreement between the *pn*QRPA and the large-basis shell model.

As we alluded in the last section, the $B(\mathrm{GT}^+)$ strength in the *pn*QRPA is spread out compared with the shell model result. This is partly related to the fact that the 1^+_m excitations constructed from the ^{46}Ti ground state in the *pn*QRPA do not have good isospin. The ^{46}Ti ground state has isospin $T = 1$. The β^- Gamow-Teller decay can go to the excitations with T =0, 1, and 2. The

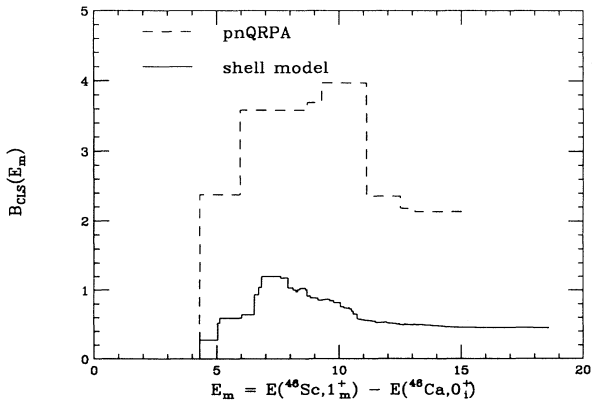

FIG. 4. Running sum of the closure $2\nu\beta\beta$ decay matrix element $B_{\mathrm{CLS}}(E_m)$ as a function of the ^{46}Sc 1^+ excitation energies relative to the ^{46}Ca ground state.

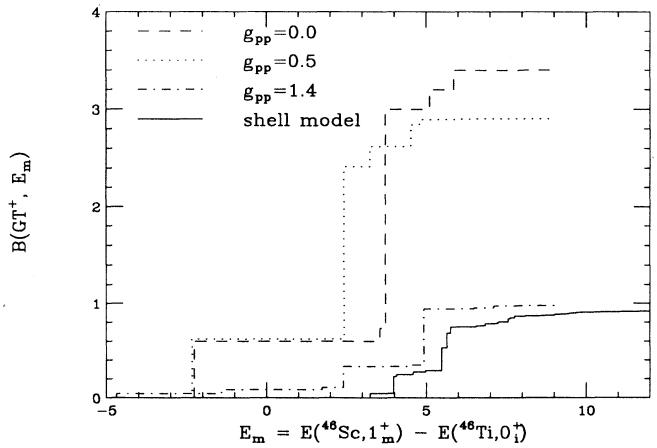

FIG. 5. Running sum of $B(\mathrm{GT}^+, E_m)$ for ^{46}Ti $\rightarrow$ ^{46}Sc in the *pn*QRPA with various g_{pp} ($g_{ph} = 1$).

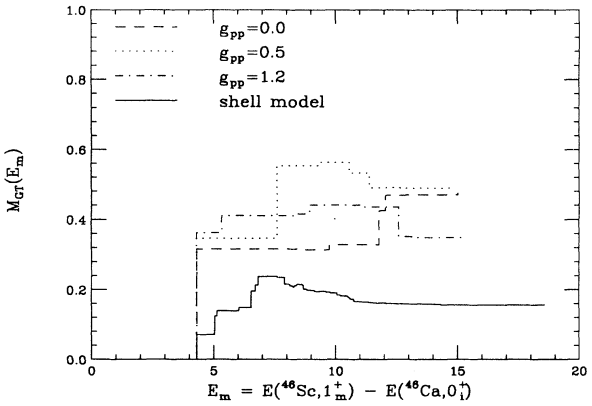

FIG. 6. Running sum of $M_{\rm GT}(E_m)$ in the pnQRPA with various g_{pp} ($g_{ph}=1$).

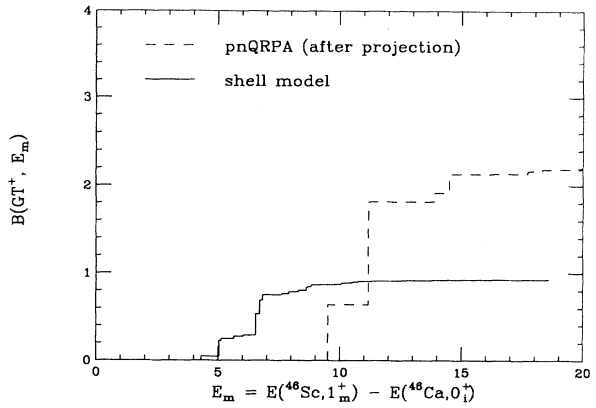

FIG. 8. Running sum of $B(\mathrm{GT}^+, E_m)$ in the pnQRPA, in which we project $B(\mathrm{GT}^+)$ onto the excitations constructed from ^{46}Ca β^- decay.

β^+ Gamow-Teller decay only go to the excitations with $T=2$. In the shell model, the excited states with various T are, of course, independent. However, in the pnQRPA, the energy spectra of the 1^+_m states in both β^- and β^+ are exactly the same. The β^- and β^+ Gamow-Teller strengths are different due to the various combination of the X and Y amplitudes [Eqs. (18) and (19)]. The consequence of this is that the lowest 1^+_m state in β^+ which should be pure $T=2$ is (due to the spurious isospin mixing) mainly from the $T=0$ 1^+_m state and hence is much to low in energy. But the $1^+_{m'}$ states constructed from the ^{46}Ca ground state have much better isospin because the β^+ Gamow-Teller decay is forbidden in the $0f1p$ shell. Thus we project the 1^+_m states obtained in the ^{46}Ti β^+ calculation onto the $1^+_{m'}$ states obtained in the ^{46}Ca β^- calculation and redefine the $M_m(\mathrm{GT}^+)$ in Eq. (17) as

$$M_m(\mathrm{GT}^+)=\sum_{m'}\langle J^\pi_{m'}||\sigma t^+||J^\pi_i\rangle\langle J^\pi_{m'}|J^\pi_m\rangle, \qquad (41)$$

where the projection factor $\langle J^\pi_{m'}|J^\pi_m\rangle$ is given by Eq. (36). The running sum $B(\mathrm{GT}, E_m)$ for the redefined $M_m(\mathrm{GT}^+)$ is shown in Fig. 8. We find that the shape of the $B(\mathrm{GT}^+)$ strength distribution is now in much better agreement with the shell model. The CTME given in Table III do not change significantly.

Another empirical improvement might be achieved by using some shell-model quasiparticle energies and/or occupation probabilities in the pnQRPA. These types of the modified models are called "hybrid" pnQRPA.

Now we introduce the shell-model quasiparticle energies. Since the BCS quasiparticle energies can be understood as the lowest excited energies of the odd nucleus [28, 30], one may appropriately analyze the odd nucleus energy spectra in the shell-model calculations, and find those excited states which are qualitatively equivalent to the single quasiparticle E_j excitations. For example, the shell-model quasineutron energies of ^{46}Ti can be obtained as follows: the one-particle transfer amplitudes are calculated between the ^{46}Ti ground state and the ^{47}Ti excited states $J=7/2^-$ (or $3/2^-$, $5/2^-$, and $1/2^-$). The eigenvalue of the state which has the largest overlap in one-particle transfer is considered as the shell-model quasineutron energy $E_{f_{7/2}}$ (or $E_{p_{3/2}}$, $E_{f_{5/2}}$, and $E_{p_{1/2}}$). The shell-model occupation probabilities are defined by Eq. (30). The shell-model occupation probabilities and quasiparticle energies for proton and neutron of ^{46}Ti are given in the Table I and compared with the BCS results.

The calculations for three types of "hybrid" pnQRPA are shown in Fig. 9. The dashed line is the pnQRPA with BCS occupations and shell-model quasiparticle energies. The dotted line is the pnQRPA with shell-model occupations and BCS quasiparticle energies. The dot-dashed line is the pnQRPA with shell-model occupations and quasiparticle energies. One finds that the total $B(\mathrm{GT}^+)$ strength is suppressed in the "hybrid" pnQRPA. That is 2.187 in the pnQRPA, 1.959 in the "hybrid" pnQRPA with the shell-model quasiparticle energies and the BCS occupation probabilities, 1.687 in the "hybrid" pnQRPA with the BCS quasiparticle energies and the shell-model occupation probabilities, and 1.335 in the "hybrid" pnQRPA with the shell-model quasiparticle energies and the occupation probabilities. The latter is close to 0.928 obtained for the total $B(\mathrm{GT}^+)$ in the large-

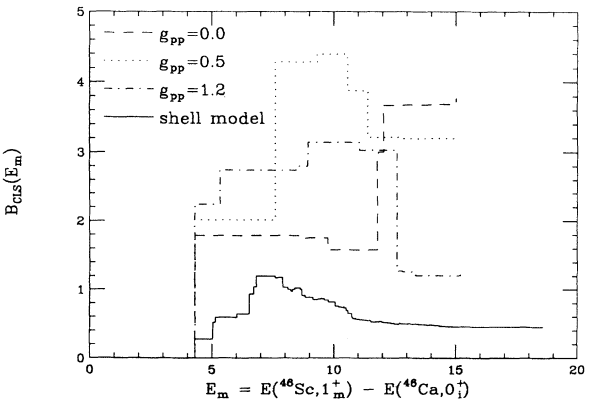

FIG. 7. Running sum of $B_{\rm CLS}(E_m)$ in the pnQRPA with various g_{pp} ($g_{ph}=1$).

basis shell model.

The "hybrid" models have not improved the strength distribution. But comparing to the shape of the spectrum of the *pn*QRPA with $g_{pp} = 1.4$ in Fig. 1, the "hybrid" *pn*QRPA with the shell-model parameters (the dot-dashed line in Fig. 9) still keeps a reasonable shape. In the "hybrid" *pn*QRPA, the position of the 1^+ state almost remains the same; i.e., it still differs by 6 MeV from the shell-model calculation.

The CTME values of the "hybrid" *pn*QRPA are presented in columns B, C, and D of Table III. The CTME in column B are obtained by using the shell-model quasiparticle energies and the BCS occupation probabilities in the *pn*QRPA. We find that the difference between columns B and E is decreased only for the transitions $f_{7/2} \rightarrow f_{7/2}$, but the CTME in other transitions become worse or remain the same. The CTME values in column C, using the BCS quasiparticle energies and the shell-model occupation probabilities, and column D, using the shell-model quasiparticle energies and the occupation probabilities, present a similar behavior. The CTME in the transition $f_{7/2} \rightarrow f_{7/2}$ now have the same sign as those in column E. The CTME for the transition $p_{3/2} \rightarrow p_{1/2}$ and $f_{5/2} \rightarrow f_{5/2}$ have been improved over those in the *pn*QRPA. But other CTME values become worse compared to those in the *pn*QRPA.

We compare the occupation factors between the BCS and shell-model in Table I and find in order to reproduce shell-model occupation factors, the pairing gap in the BCS equation should be unrealistically increased to around 4 MeV [21]. It requires a very strong and unrealistically effective interaction. The present BCS gaps are around 1 MeV.

Encouraged by the successes of the improvements of the *pn*QRPA we also consider the use of "hybrid" models for the $\beta\beta$ decay matrix elements. The shell-model quasiparticle energies and occupation probabilities for the initial and final nuclei are given in Table I and Table II. In Fig. 10, the solid line is from the shell model, the dashed line is from using the shell-model quasiparticle energies in the *pn*QRPA, the dotted line from using the shell-model occupation numbers, and the dash-dotted line from using shell-model quasiparticle and occupation

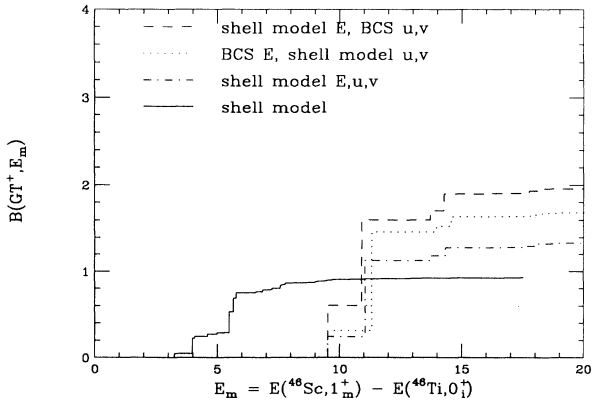

FIG. 9. Running sum of the Gamow-Teller strength $B(\mathrm{GT}^+, E_m)$ in the "hybrid" *pn*QRPA.

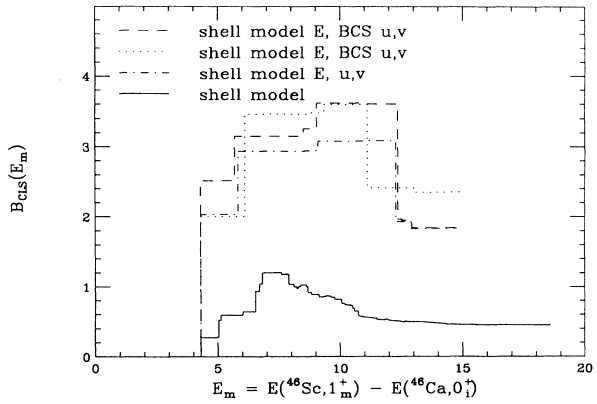

FIG. 10. Running sum of $B_{\mathrm{CLS}}(E_m)$ in the "hybrid" *pn*QRPA.

probabilities. We find that the "hybrid" *pn*QRPA cannot give enough suppression for total B_{CLS} to reproduce the shell-model results. One may conclude the "hybrid" models do not work well for $2\nu\beta\beta$ decay.

V. SUMMARY AND CONCLUSIONS

The nuclear shell model and the *pn*QRPA equation are very important nuclear structure theories for studying β and $\beta\beta$ decays. But the approach of these two models is different. Many or all types of many-body correlations are taken into account in the large-basis shell-model calculations. The *pn*QRPA is an approximate model, which includes only some special classes of the correlations. The goal of this paper was to examine the validity and accuracy of the *pn*QRPA for β^+ and $\beta\beta$ processes. The examination is achieved by making a comparison of the *pn*QRPA and the large-basis shell-model calculations in the $0f1p$ shell.

In Sec. II, the BCS and *pn*QRPA have been developed. The input ingredients in the BCS and *pn*QRPA are the same as those in the shell model, namely, the bare single-particle energies at the closed shell and two-body interaction matrix elements. Therefore there is no free parameter for both models in our comparison. The coherent transition matrix elements (CTME) are introduced for analysis of the single-particle state contributions in β decay. In Sec. III, we have investigated the accuracy of the *pn*QRPA approach to β and $\beta\beta$ decays. Comparisons of the *pn*QRPA and large-basis shell-model calculations for nuclei with A=46 have been made. Our comparisons have shown the *pn*QRPA overestimates the total $B(\mathrm{GT}^+)$ and $\beta\beta$ decay matrix elements, and there are large discrepancies in the shapes of the strength distributions between the *pn*QRPA and shell-model calculations. The CTME of the *pn*QRPA are also in poor agreement with those of the shell model. Thus we may conclude there must be some correlations which are important to β and $2\nu\beta\beta$ decay but have not been included in the *pn*QRPA.

Two types of empirical improvement for the *pn*QRPA were suggested in Sec. IV. One was to project the β^+

energy spectra onto the β^- spectra in order to have relatively good isospin. The shape of the strength distribution after projection is close to the shell-model result. Another was the "hybrid" *pn*QRPA, which was obtained by using the shell-model occupation probabilities and the shell-model quasiparticle energies in the *pn*QRPA. About 50% suppressions are found for the total $B(\mathrm{GT}^+)$ strength. The shape of the $B(\mathrm{GT}^+)$ distribution has not been improved but it is more reasonable than that in the *pn*QRPA with larger g_{pp} values. But for $2\nu\beta\beta$ decay, we find the "hybrid" *pn*QRPA does not work very well. The Gamow-Teller β^+ strength and double-beta decay matrix element in medium and heavy nuclei will continue to be a challenge for nuclear structure models.

ACKNOWLEDGMENTS

We would like to thank Dr. A. Sustich and Dr. D. Cha for their helpful discussions. This work was supported by the National Science Foundation under Grant No. PHY-9017077.

APPENDIX

In this Appendix, we will introduce and discuss the coherent one-body transition density and coherent transition matrix element. In the second-quantization formalism, the one-body operator can be expressed by

$$F = \sum_{\alpha\beta} \langle \alpha | F | \beta \rangle a_\alpha^\dagger a_\beta, \tag{A1}$$

where $|\alpha\rangle$ and $|\beta\rangle$ are the single-particle states. The transition matrix element between the initial state $|i\rangle$ and the final state $|f\rangle$ is given by

$$M_{fi} = \langle f | F | i \rangle = \sum_{\alpha\beta} \langle \alpha | F | \beta \rangle \langle f | a_\alpha^\dagger a_\beta | i \rangle. \tag{A2}$$

$\langle \alpha | F | \beta \rangle$ is called the single-particle matrix element (SPME) which is only related to the single-particle states $|\alpha\rangle$ and $|\beta\rangle$. $\langle f | a_\alpha^\dagger a_\beta | i \rangle$ is called the one-body transition density (OBTD), which is the function of the initial and final states as well as the single-particle states $|\alpha\rangle$ and $|\beta\rangle$. Then Eq. (A2) can be rewritten as

$$M_{fi} = \sum_o \mathrm{SPME}(o)\mathrm{OBTD}(o, f, i), \tag{A3}$$

where o represents the single-particle states.

Now we introduce a *coherent state* $|C\rangle$ which is defined by

$$|C\rangle = N_C F |i\rangle, \tag{A4}$$

where N_C is the normalization factor which is determined by

$$\begin{aligned} \langle C | C \rangle &= N_C^2 \langle i | F^\dagger F | i \rangle \\ &= N_C^2 \sum_f \langle i | F^\dagger | f \rangle \langle f | F | i \rangle. \end{aligned} \tag{A5}$$

Then we have

$$N_C = \frac{1}{\sqrt{\sum_f \langle f | F | i \rangle^2}}. \tag{A6}$$

The transition matrix element between the coherent state and initial state is

$$\begin{aligned} \langle C | F | i \rangle &= N_C \langle i | F^\dagger F | i \rangle \\ &= N_C \sum_f \langle i | F^\dagger | f \rangle \langle f | F | i \rangle \\ &= N_C \sum_{o,f} M_{fi} \mathrm{SPME}(o)\mathrm{OBTD}(o, f, i) \\ &= \sum_o \mathrm{SPME}(o)\mathrm{COBTD}(o, i) \\ &= \sum_o \mathrm{CTME}(o, i). \end{aligned} \tag{A7}$$

where the COBTD and CTME are the *coherent one-body transition density* and *coherent transition matrix element* which are defined by

$$\begin{aligned} \mathrm{COBTD}(o, i) &= N_C \sum_f M_{fi} \mathrm{OBTD}(o, f, i) \\ \mathrm{CTME}(o, i) &= \mathrm{SPME}(o)\mathrm{COBTD}(o, f, i). \end{aligned} \tag{A8}$$

The COBTD and CTME are a function of the single-particle state and initial state. It represents the single-particle state effects in the total transition strength and depends only on the structure of the initial state.

[1] P.J. Brussaard and P.W.M. Glaudemans, *Shell Model Applications in Nuclear Spectroscopy* (North-Holland, Amsterdam, 1977).
[2] M. Morita, *Beta Decay and Muon Capture* (Advanced Book Program, Reading, Massachusetts, 1973).
[3] W.C. Haxton and G.J. Stephenson, Prog. Part. Nucl. Phys. **12**, 409 (1984).
[4] M. Doi, T. Kotani, and E. Takasugi, Prog. Theor. Phys. Suppl. **83**, 1 (1985).
[5] K. Muto and H.V. Klapdor, in *Neutrinos*, edited by H.V. Klapdor (Springer-Verlag, Berlin, 1988).
[6] J.D. Vergados, Phys. Rep. **133**, 1 (1986).
[7] S.R. Elliott, A.A. Hahn, and M.K. Moe, Phys. Rev. Lett. **59**, 2020 (1987).
[8] F.T. Avignone III *et al.*, Phys. Lett. B **256**, 559 (1991).
[9] H. Ejiri *et al.*, Phys. Lett. B **258**, 17 (1991).
[10] A.L. Turkevich, T.E. Economou, and G.A. Cowan, Phys. Rev. Lett. **67**, 3211 (1991).
[11] B.A. Brown and B.H. Wildenthal, Annu. Rev. Nucl. Part. Sci. **38**, 29 (1988).
[12] J.A. Halbeib and R.A. Sorensen, Nucl. Phys. **A98**, 542 (1967).
[13] D. Cha, Phys. Rev. C **27**, 2269 (1983).
[14] P. Kleinheinz *et al.*, Phys. Rev. Lett. **55**, 2664 (1985).
[15] J. Suhonen, A. Faessler, T. Taigel, and T. Tomoda, Phys. Lett. B **202**, 174 (1988); J. Suhonen, T. Taigel, and A. Faessler, Nucl. Phys. **A486**, 91 (1988).
[16] P. Vogel and M.R. Zirnbaur, Phys. Rev. Lett. **57**, 3148 (1986).
[17] O. Civitarese, A. Faessler, and T. Tomada, Phys. Lett.

B **194**, 11 (1987).
[18] J. Engel, P. Vogel, and M.R. Zirnbauer, Phys. Rev. C **37**, 731 (1988).
[19] K. Muto, E. Bender, and H.V. Klapdor, Z. Phys. A **333**, 125 (1989); **334**, 177 (1989); **334**, 187 (1989).
[20] M. Hirsch *et al.*, Nucl. Phys. **A535**, 62 (1991).
[21] B. Lauritzen, Nucl. Phys. **A489**, 237 (1988).
[22] B.A. Brown and L. Zhao, in *Nuclear Weak Process and Nuclear Structure*, edited by A.M. Morita *et al.* (World Scientific, Singapore, 1989), p. 291.
[23] O. Civitarese, H. Müther, L.D. Skouras, and A. Faessler, J. Phys. G **17**, 1363 (1991).
[24] N. Auerbach, G.F. Bertsch, B.A. Brown, and L. Zhao (submitted to Nucl. Phys. A).
[25] K. Muto, E. Bender, and H.V. Klapdor, Z. Phys. A **339**, 435 (1991).
[26] E. Caurier, A. Poves, and A. P. Zuker, Phys. Lett. B **252**, 13 (1990).
[27] L. Zhao, B.A. Brown, and W.A. Richter, Phys. Rev. C **42**, 1120 (1990).
[28] D.J. Rowe, *Nuclear Collective Motion* (Methuen, London, 1970).
[29] P. Ring and P. Schuck, *The Nuclear Many-Body Problem* (Springer-Verlag, New York, 1980).
[30] R.D. Lawson, *Theory of the Nuclear Shell Model* (Clarendon Press, Oxford, 1980).
[31] B.A. Brown and R. Sherr, Nucl. Phys. **A322**, 61 (1979).
[32] A. Etchegoyen, W.D.M. Rae, N.S. Godwin, W.A. Richter, C.H. Zimmerman, B.A. Brown, W.E. Ormand, and J.S. Winfield, MSU-NSCL Report No. 524, 1985.
[33] K. Grotz and H.V. Klapdor, Nucl. Phys. **A460**, 395 (1986).
[34] W.A. Richter, M.G.V.D. Merwe, R.E. Julies, and B.A. Brown, Nucl. Phys. **A523**, 325 (1991).
[35] B.A. Brown and L. Zhao, in *Understanding the Variety of Nuclear Excitations*, edited by A. Covello (World Scientific, Singapore, 1990), p. 497.
[36] T. Tsuboi, K. Muto, and H. Horie, Phys. Lett. **143B**, 293 (1984).